Brain Tissue Segmentation using T1-weighted MRI scans

Pepe Cano-Manuel Claver
Universiteit Utrecht
j.l.cano-manuelclaver@students.uu.nl
7272627

Raquel González López
Universiteit Utrecht
r.gonzalezlopez@students.uu.nl
4860551

Ana San Román Gaitero
Universiteit Utrecht
a.sanromangaitero@students.uu.nl
9918647

***Abstract*—The segmentation of T1-weighted MRI brain images is done using a unique approach that is presented in this research. The MRI scan, the most recent image segmentation methods, and each method's issues are briefly discussed in the first section. The second section then gives an overview of the dataset, the MRI preprocessing procedures, and the pipeline that was selected for brain segmentation. The third part also includes a display of the outcomes of the suggested methodology. The discussion and conclusion of the results of image segmentation are presented in parts four and five.**

***Index Terms*—MRI segmentation, Image segmentation, Fuzzy Method,**

I. Introduction

In many clinical applications, image segmentation is the first and most critical step in medical image analysis.

As part of brain magnetic resonance imaging (MRI) analysis, image segmentation is frequently used to visualize anatomical brain structures, analyze brain changes, delineate pathological regions, plan surgery, and perform image-guided interventions [1]. This is due to the inherent characteristics of anatomical MRI, featuring excellent soft tissue contrasts that are based on multiple contrast parameters, the ability to image in oblique orientations, and the capability to provide two-dimensional (2D) as well as three-dimensional (3D) data. MRI is considered a non-invasive diagnostic imaging modality that generates cross-sectional images of the human body without the use of ionizing radiation [2].

In MRI, images are formed by applying a large static magnetic field to hydrogen particles, which results in a perturbation of their proton's magnetic moments. MRI's signal is formed during the relaxation process which entails the returning time of these magnetic moments to their equilibrium state. The strength and duration of the signal, induced in the relaxation process, depend on (i) the proton density, (ii) the time which describes how fast the net magnetization takes to relax back to its equilibrium (T1), and (iii) the time where magnetization components decrease to zero (T2) [3]. Therefore, different MRI pulse sequences generate different patterns of tissue contrast.

In this sense, brain tissue segmentation on MRI images is a challenging clinical matter due to the variation in brain shapes and the similarity in intensity values between the brain and non-brain tissues. Generally, MRI is the most common technique for brain tissue research as its capable of obtaining high soft tissue contrast with a T1-weighted image [4]. The brain MRI image segmentation method mainly refers to background removal, skull stripping, and the partitioning of brain tissue, which can be divided into white matter (WM), gray matter (GM), and cerebrospinal fluid (CSF). All these segmentation outcomes provide a basis for medical image registration, 3D reconstruction, and visualization [5].

Nowadays, brain image segmentation has been performed using a variety of image techniques. Traditional image segmentation methods include thresholding, clustering-based methods, region-based methods, edge-based methods, active contours, and surface methods [3]. Some studies have proposed a solution for brain tissue segmentation by fuzzy clustering algorithms where the traditional fuzzy c-means (FCM) clustering is upgraded to an improved algorithm which uses a view weight adaptive learning mechanism so that each view obtains the optimal weight according to its cluster contribution [5]. Meanwhile, others have improved FCM to an enhanced fuzzy relaxation approach [6]. Other studies have applied a region growing on a rough brain image obtained by the binarization of the image using a determined threshold intensity [7] obtaining precise results. Hence, there are a considerably large amount of studies that have come up with a variety of different pipelines using the traditional tools mentioned above.

Nevertheless, these traditional segmentation techniques of MRI images come across a diversity of difficulties. These problems include the partial volume which entails the contribution of the same voxel in multiple tissue types. Besides, the bias field effect, which relates to the presence of smoothly varying intensities inside tissues, can greatly degrade the accuracy of further analysis steps [8]. Lastly, different kinds of noise have varying degrees of impact on the image [9, 3].

Currently, there are a fair amount of software packages available that have been developed to address the problem of creating head segmentations from T1 structural MRIs [4]. Some of these packages include $BrainSuite$[1], $Freesurfer$[2], $FSL\ BET/FAST$[3][4], SPM[5] which are easy-to-use interfaces that perform data processing, analysis, and visualization of brain MRI data.

On the other hand, a less traditional tool which is emerging for automatic image segmentation is machine learning. Machine learning makes use of known labels of the image segmentation as well as different features such as intensity and texture, which help obtain a more accurate segmentation [4]. However, effectively building and deploying artificial intelligence and machine learning systems require large datasets which are not available for this kind of task since manual segmentations from a clinical expert are not abundant.

Therefore, the aim of this report is to obtain the segmentation of the WM, GM, CSF, skull, and background of the MRI images provided by some of the traditional image segmentation tools mentioned above and to address the complexity and challenges of the brain MRI segmentation problem.

The present report introduces a novel approach for the segmentation of T1-weighted MRI brain images. This first section introduces a brief summary of the MRI scan, the current image segmentation techniques, and their respective problems. Next, the second section presents a description of the dataset, the MRI preprocessing steps, and the chosen pipeline for brain segmentation. Furthermore, in the third section, the results obtained under the proposed methodology are shown. The fourth and fifth sections of a discussion and conclusion of the image segmentation outcomes.

II. Materials and Methods

This section begins by describing the provided dataset and its respective image characteristics. Subsequently, this section continues explaining the chosen image segmentation pipeline, starting with preprocessing, followed by background removal, brain tissue segmentation, and skull stripping. The proposed algorithm was developed and implemented in MATLAB R2021a[6].

A. Dataset

The provided dataset contains a total of 15 2D MRI images of the human brain. These are T1-weighted images that have been acquired with a gradient-echo sequence, displaying excellent contrast between brain tissues. Moreover, the dataset contains three spatial orientations, including axial, coronal, and sagittal as seen in Fig. 1. Each plane counts with 5 different images which represent different parts of the brain. All images are provided in a *.mat* file with its corresponding pixel values as float numbers. Each image is composed of 43,200 pixels (240x180), except for the sagittal orientation which is composed of 57,600 pixels (240x240). All ranging from 0 to a different maximum value depending on the image.

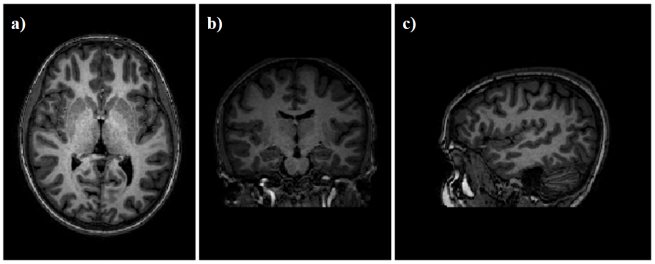

Fig. 1. Example of three T1-weighted images from an a) axial, b) coronal, and c) sagittal view

B. Preprocessing

Several preprocessing steps were applied to the original images to eliminate unwanted distortions and improve specific characteristics, and in this way, make the image fit for further analysis. These steps include noise reduction and bias intensity inhomogeneities removal.

One of the most common issues in MRI is noise. Speckle noise, Gaussian noise, and salt-and-pepper noise are common sources of noise that can degrade the quality of an MRI image [10]. For this reason, the first step consisted of applying an averaging filter, with a window size of 3x3. The $filt_average$ function was used, which included the $fspecial$ function to define the default averaging filter and the $imfilter$ function, both from MATLAB, to apply it to the desired image. In this way, additive noise caused by image acquirement or transmission in the images could be reduced [11]. In general terms, the averaging filter maintains a good image quality, especially if speckle noise is present[9].

Another potential confounder is the presence of a low-frequency intensity nonuniformity present in the image data also known as bias, inhomogeneity, illumination nonuniformity, or gain field. The piecewise constant property of medical images is invalidated by this effect since it results in variations in the intensity of the same tissue at various points within the image [8]. A widely used state-of-the-art method to correct this is the N4 bias correction [12]. It is an iterative method that searches for the smooth multiplicative field that maximizes the high-frequency content of the tissue intensity distribution. For this, the $Run4ANTS$ function was used.

[1]http://brainsuite.org/
[2]https://surfer.nmr.mgh.harvard.edu/
[3]https://fsl.fmrib.ox.ac.uk/fsl/fslwiki/BET
[4]https://fsl.fmrib.ox.ac.uk/fsl/fslwiki/FAST
[5]https://www.fil.ion.ucl.ac.uk/spm/software/
[6]https://nl.mathworks.com/products/matlab.html

C. Background Removal

The first section removed was the background from the head of the patients.

The images provided present some noise between the skull and the background that alters the segmentation. Following Fig. 2, can be appreciated that they are randomly positioned small dots. For removing them, a specific prepossessing is applied which is only used in this section: low pass filter using Fourier transform (FT).

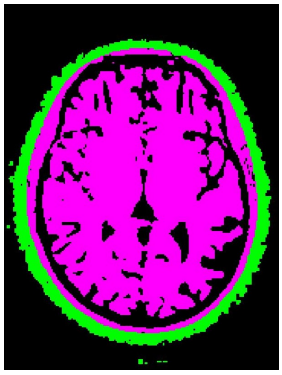

Fig. 2. Axial image. In green, the noise surrounding the skull; in purple, the head area without the noise.

The 2D FT provides details about the image's frequency composition, where MxN represents the size of the image in the real domain.

$$F(u,v) = \sum_{m=0}^{M-1} \sum_{n=o}^{N-1} f(m,n) e^{j2\pi(\frac{um}{M} + \frac{vn}{N})} \tag{1}$$

As can be seen in equation 1, its definition uses both complex and real components, so the resulting transform generates two images. [13] Out of them, the magnitude (real) image groups the frequency components concentrically, that is, higher frequencies in the periphery and lower frequencies in the middle. In this sense, high frequencies are related to small and noisy dots and the edges of the images. Therefore, a circular mask was applied removing the high-frequency components of the images.

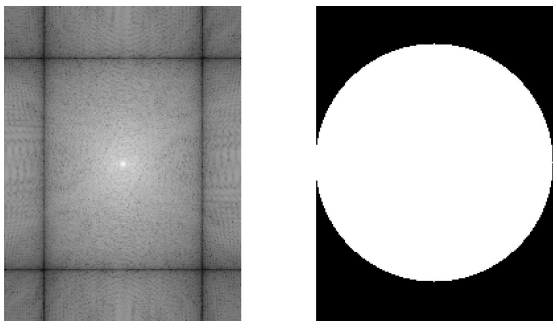

Fig. 3. To the left, 2D FT of an axial image. To the right, the applied mask with a radius half of the size of the smallest side of the image.

The function $LP\_fourier$ provided was used for the low pass filtering of the images using FT. It includes the MATLAB functions $ifft2$ and $fft2$.

Once the images' noise around the skull was removed, the background pixels needed to be detected. For that, the characteristic low intensity of the pixels present in the background is considered. Therefore, the Otsu method was used.

The Otsu thresholding (afterward Otsu) is an automatic image segmentation method. The method outputs a single threshold of intensity that divides pixels into the foreground and background classes. This threshold is established through maximization of inter-class variance or, equivalently, minimization of intra-class intensity variance [14].

In this sense, due to the large amount of pixels present in the background with values similar to 0, the first Otsu segmentation divided the image between the background and the head. The implementation was carried out using *graythresh* MATLAB function within the *otsu* function provided.

However, the pixels within the head that had similar values than the background were removed too. To ensure that the head mask results in a compact, uniform, and hole-less structure a closing operation (CO) was used.

The CO is a type of morphological operation utilized to remove small holes. It is performed by a dilation followed by an erosion. Dilation is used to convolute a kernel of ones, and defined length and structure, through all the pixels of the images. This operation increases the size of the object. On the other hand, erosion is the inverse operation [15].

Since the structures of the brain do not follow any particular pattern, e.g., rectangular patterns, the structuring element used for closing was a circle of known radius. To parameterize the radius the following relation is used, where N is the radius factor.

$$radius = round(\frac{image \quad size \cdot N}{240x240}) \tag{2}$$

Where N is the assigned radius factor that is common for all the images introduced within the algorithm. For this previous closing the N was of 60.

D. Brain Tissue

The next step of brain image segmentation is the division of brain tissue into three different parts: WM, GM, and CSF. To approach this problem several steps are followed beginning with a preparation of the brain mask and finalizing with a clustering method able to acquire the brain tissue segmentation.

Firstly, an erosion to the image obtained after the Otsu was applied.

In case the images given are not cropped, in other words, present a lot of pixels in the background that could alter the N factor, the function *crop_im* is provided. It crops the images in the until a non-zero pixel is found on each one of the four directions. The function is not used in our proposed method for the sake of optimizing the timing. However, it can be used in case it is known that the images have a huge amount of background or zero-padding, but our team did not know if that is a common practice. This function crops in the four directions until a non-zero value is found.

In this regard, the erosion applied is of N=2. Then, a the maximum connected region method is used, utilizing the MATLAB function *bwconncomp*. This provides the 4 bigger connected regions of the image. Thanks to the erosion, the brain is separated from the skull (see Fig. 4). And with the maximum connected region the brain is obtained as the biggest region provided.

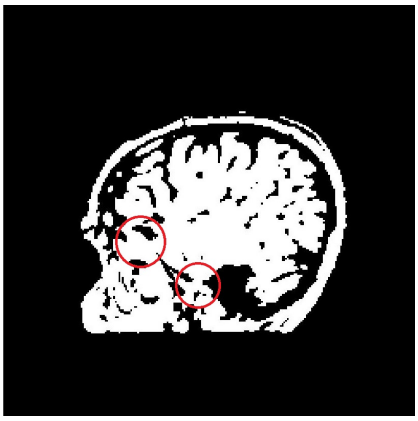

Fig. 4. Coronal image where the brain is connected to the skull right after the Otsu, the red circles indicate those areas.

Subsequently, a dilation of the same factor (N=2) is applied to compensate the previous erosion. At last, a closing is carried out, using the provided function *opt_closing*, which is based on the MATLAB *imclose* function. The function increases the radius in steps of ones until all the holes of the images are closed. It is used to obtain the final brain mask capable of segmenting the whole brain from the other non-brain tissues.

Finally, the fuzzy c-means (FCM) clustering algorithm is applied to the segmented brain, image visualized in Fig. 5, for the segmentation of the brain tissues.

The FCM clustering is a efficient classification method which allows each pixel to belong to multiple classes according to a certain membership value [1]. FCM is based on minimizing an objective function as follows [1, 16]:

$$J_m = \sum_{i=1}^{C}\sum_{j=1}^{N} u_{ij}^m D_{ij}, \tag{3}$$

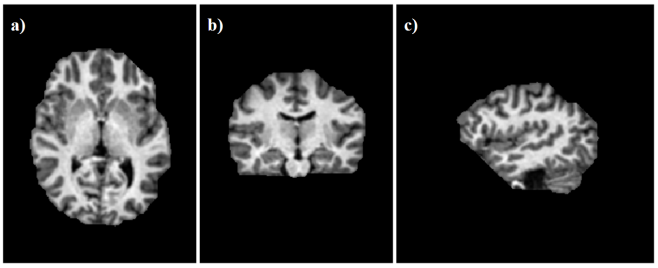

Fig. 5. Example of three "brain" images that will be introduced as an input for the FCM algorithm from an a) axial, b) coronal, and c) sagittal view

where N is the number of elements in the image that need to be clustered, m controls the fuzziness degree of clustering, u_{ij} is the membership function of the element x_j belonging to cluster i, and D is the distance between data x_i and center of the cluster v_i. The membership function x_j satisfies the following three conditions: $u_{ij} \in [0, 1]$, $\sum_{i=1}^{C} u_{ij} = 1$ and $0 < \sum_{j=1}^{N} u_{ij} < N$.

In the iterative process, the clustering centres and membership degrees are always updating, meanwhile, the value of objective function is closer to the minimum value. The membership matrix updates and the cluster centres by the following formula:

$$u_{ij} = [\sum_{k=1}^{C}(D_{ij})/D_{kj})^{\frac{1}{m-1}}]^{-1} \tag{4}$$

$$v_j = \frac{\sum_{j=1}^{N} u_{ij}^m x_j}{\sum_{j=1}^{N} u_{ij}^m} \tag{5}$$

Therefore, FCM optimizes the objective function updating the membership value u_{ij} and the center of each cluster v_j.

E. Skull stripping

Once the brain (containing white matter, gray matter, and CSF) and the background were obtained, the skull was computed as the remaining of superposing all those elements.

F. Quantitative assessment metrics

To evaluate the model performance, there are several quantitative evaluation approaches. The Jaccard similarity (JS) is a metric that evaluates the segmentation accuracy [**empty citation**]. It is defined as the fraction between the conjunction and disjunction of the ground truth (O_1) and the segmented images (O_2).

$$JS = \frac{O_1 \cap O_2}{O_1 \cup O_2}, \tag{6}$$

It gives a value between 0 and 1, the greater the number the better match with the ground truth [17].

Another approach is the Dice similarity coefficient (DSC), which is a spatial overlap index and a reproducibility validation metric.

$$DSC = \frac{2 \cdot TPV}{2 \cdot TPV + +FPV + FNV}, \tag{7}$$

where TPV is the True Positive Value, TNV is True Negative Value, FPV is False Positive Value and FNV is False Negative Value. It also ranges between 0 and 1, being this last a total overlap between the ground truth and the segmented image [18].

Another three important metrics to consider are accuracy, specificity, and recall [6]:

- **Accuracy**: accuracy is the ratio among correctly identified pixels to the overall identified pixels

$$Accuracy = \frac{TPV + TNV}{TPV + TNV + FPV + TNV} \tag{8}$$

- **Specificity**: specificity is the capability to classify the non-tissue portions accurately in the resultant segmented image

$$Specificity = \frac{TNV}{TNV + FPV} \tag{9}$$

- **Recall or sensitivity**: recall indicates the capability to categorize the tissue portions accurately in the resultant segmented image

$$Recall = \frac{TPV}{TPV + FNV} \tag{10}$$

III. Results

In this section, the results for each of the methodology steps are presented.

A. Preprocessing

As exposed in the methods section, there are different types of noise or artifacts that could be presented in medical images due to acquisition or transmission errors. In Fig. 6, the results for both the noise reduction and bias field correction can be visualized.

The effect of the N4 Bias Correction algorithm can be visualized in Fig. 7. By visual comparison, it can be difficult to distinguish between the image without the bias field correction and the one with it, but subtracting both images provides a clearer visualization.

B. Background Removal

For removing the background, an additive step on preprocessing was done using the mentioned low pass filter FT, but this step was not carried out for the following segmentation of the brain.

First, the mentioned filter prevent high-frequency (noise) dots around the skull, as shown in Fig. 2. Indeed,

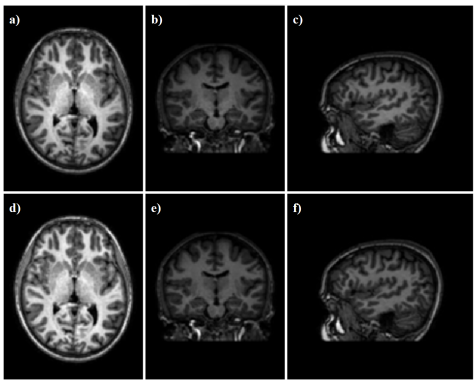

Fig. 6. Example the preprocessing steps. First noise reduction with the averaging filter for a) axial b) coronal, and c) sagittal views. Second, bias field correction with the N4 Bias Correction algorithm for a) axial b) coronal, and c) sagittal views.

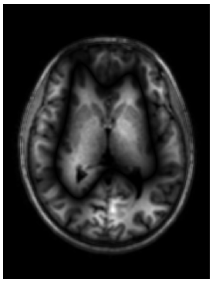

Fig. 7. Substraction of the non-corrected image and the bias field corrected image using N4 Bias Correction.

images a, b and c, on Fig. 8 show the background segmentation without applying the FT filter.

Secondly, an closing of N=30 was used to fill the holes within the mask (Fig. 8 d, e, f) giving the final background segmentation (Fig. 8 g,h,i).

However, depending on the radius of use (N factor) for the closing certain differences in the structures included in the head appear (Fig. 9).

C. Brain Tissue

For obtaining the brain mask and the segmentation of the three brain tissues under study, morphological operations and a clustering algorithm were applied. Firstly, Fig. 10 shows the results after the implementation of the morphological operators for the three planes under study. Therefore, in Fig. 10, images (a) show the outcome erosion calculated on the Otsu thresholding (Images d, e, f in Fig. 8) mask which was previously obtained in the background removal process. On the other hand, images (b) show the results of applying a dilation on the erosion images. Meanwhile. images (c) show the optimal brain mask after implementing a closing operation to the dilated images.

For some images, the erosion was not optimal, which can be seen in Fig. 11. In the left image, the radius of the

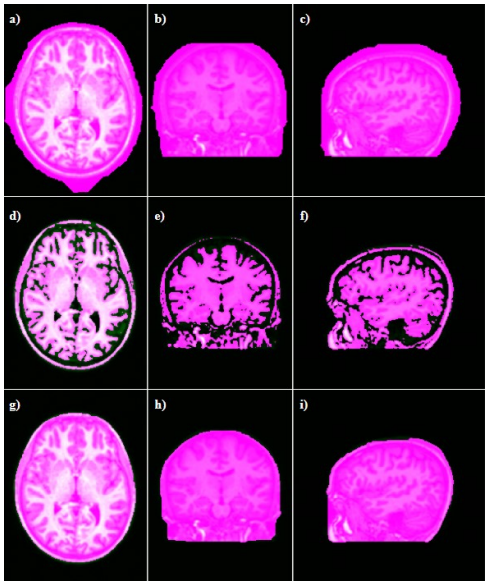

Fig. 8. Images a), b), and c) represent the background segmentation without applying the low pass FT on the three planes of study. The following d), e), and f) correspond to the three sagittal, axial, and coronal planes background segmentation without using the closing morphological operation. The last g), h), and i) show the correct background segmentation after all the steps.

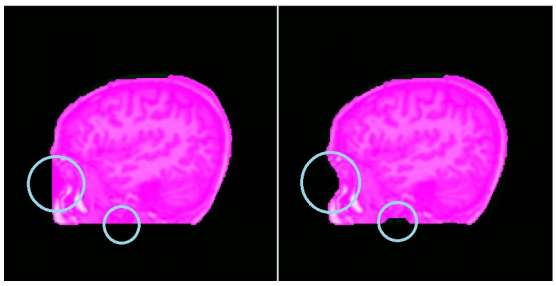

Fig. 9. To the left, Otsu images closed with a bigger radius (N=30) than the image to the right (N=10).

erosion separated brain hemispheres. In the right image, the erosion operation was not able to divide the skull from the brain tissue.

After obtaining the brain mask, the segmentation of the WM, GM, and CSF was implemented. As mentioned before, the FCM algorithm was the chosen method to overcome this challenge. The images which were introduced to the clustering function were those in Fig. 5 obtained by the brain mask. Hence, images (c), (d), and (e) in Fig. 13 and Fig. 14 show the results of the brain tissue segmentation with their respective binary masks for the three planes under study.

In Fig. 12, the FCM segmentation can be visualized. The brainstem can be clearly seen and segmented as WM, as well as the CSF.

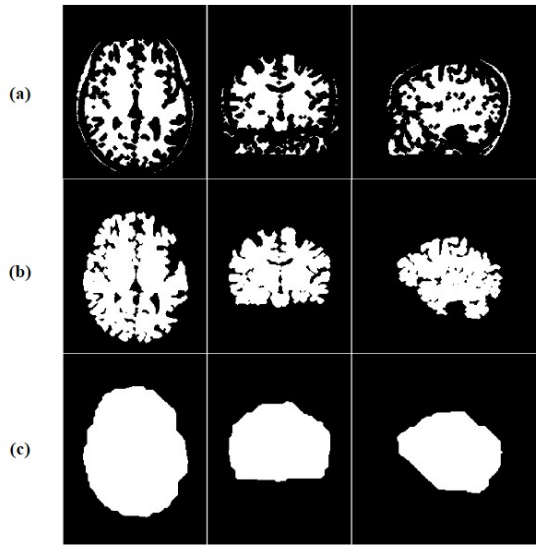

Fig. 10. Images a), b), and c) represent the outcome results after the respective morphological operators applied, being a) erosion, b) dilation, and c) closing respectively, for the three planes of study. Images c) correspond to the final brain mask for segmentation.

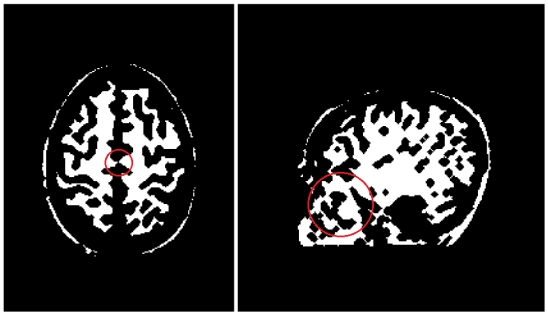

Fig. 11. Example of two images where an erosion morphological operator was applied. To the left, axial view where the two brain hemispheres are not connected, and to the right, sagittal view where the brain tissue is connected to the skull in two regions.

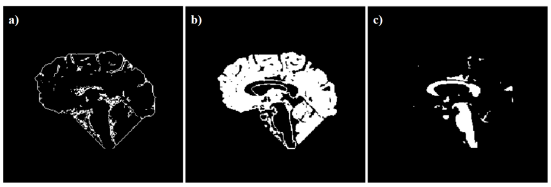

Fig. 12. MRI brain tissue segmentation using FCM algorithm. Segmentations are presented as binary masks for the sagittal view. (a) CSF segmentation, (b) WM segmentation, and (c) GM segmentation. Images a), b), and c) represent the outcome result.

D. Skull Stripping

Finally, the skull stripping is the result of subtracting the brain (containing the three main brain tissues) and background mask to the original image. It can be seen in the images a and b in Fig. 13 and Fig. 14.

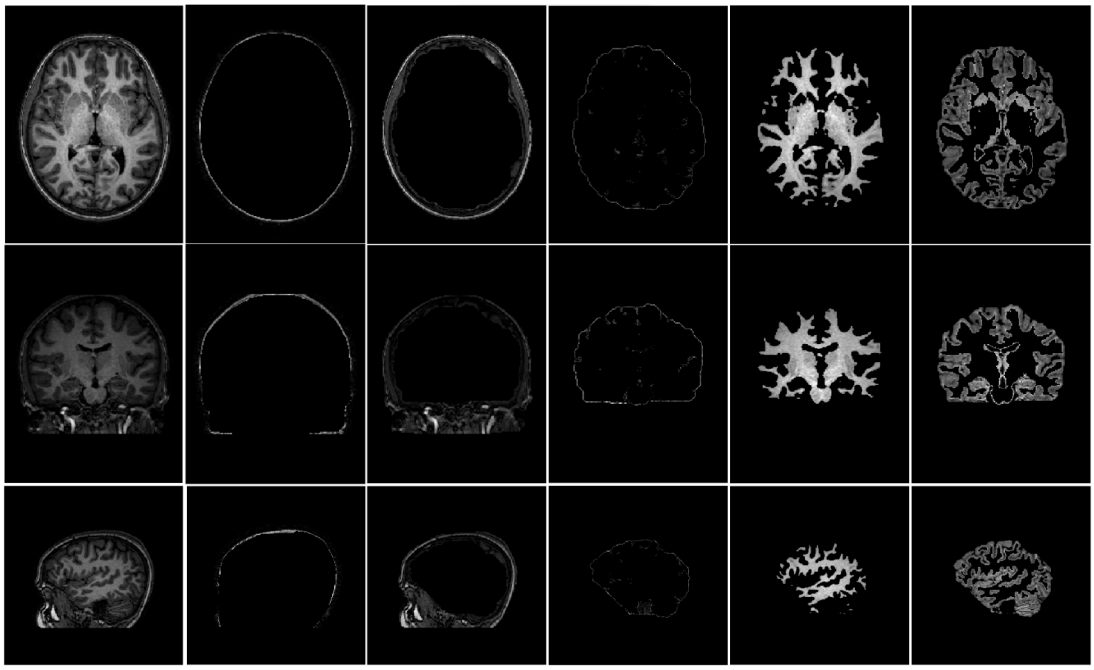

Fig. 13. MRI brain tissue segmentation using FCM algorithm. Segmentations were multiplied by the input image. First column (a): original image (b): background; second column: (c) skull stripping; third column (d): segmented CSF; fourth column (e): segmented WM; and fifth column (f): segmented GM. First row: axial view; second row: coronal view; and third row: sagittal view.

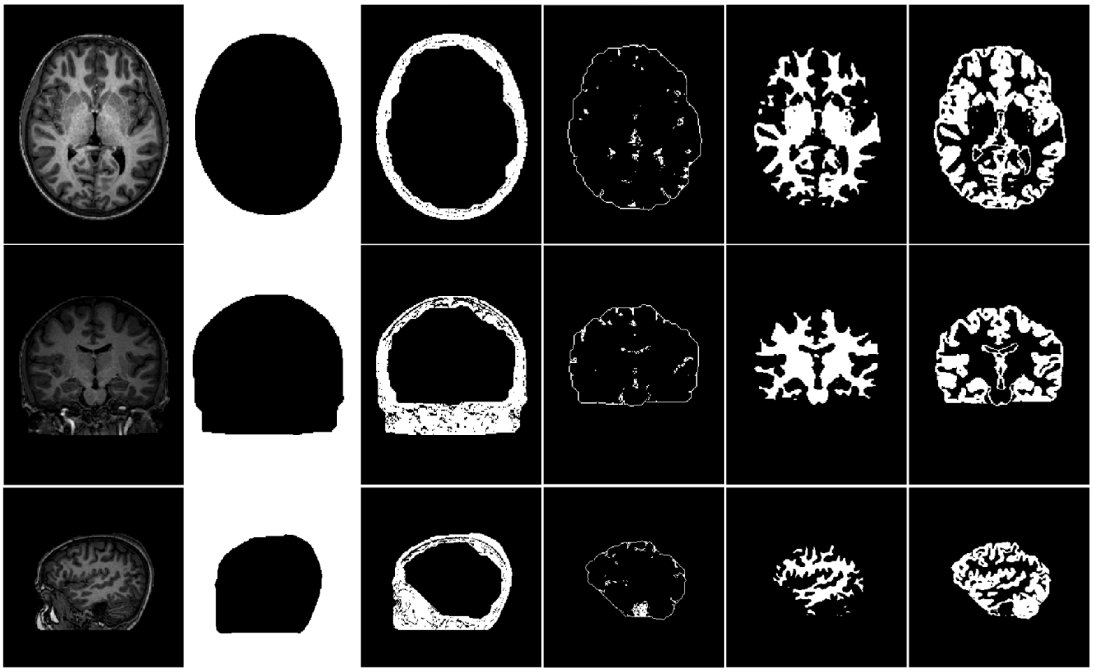

Fig. 14. MRI brain tissue segmentation using FCM algorithm. Segmentations are presented as binary masks. First column (a): original image (b): background; second column: (c) skull stripping; third column (d): segmented CSF; fourth column (e): segmented WM; and fifth column (f): segmented GM. First row: axial view; second row: coronal view; and third row: sagittal view.

IV. Discussion

The original images from the dataset provided (Fig. 6)) do not present considerable distortions or artifacts.

Firstly, the noise surrounding the skull was removed(Fig.4), which worked properly on all the images. Later, the bias field effect was properly corrected, which worked for all of the images too. Indeed, Fig. 7 demonstrates the importance of this process.

After the preprocessing, the removal of the background is carried out. It showed a proper classification of the images into background and foreground (head).

The Otsu thresholding alone gives an inaccurate estimation of the background (Fig. 8 a, b, and c) due to the presence of noise around the skull (Fig. 2). However, the use of the FT and a low pass filter mask works as a noise reduction technique, and the skull is contoured correctly (Fig. 8 d, e, and f).

Then, to ensure that the holes within the head are filled the N=60 closing technique has a proper performance. This technique allows us to prevent excessive use of the radius of the structuring element, and so an incorrect contouring of the skull against the background (Fig. 8 g, h, and i).

Nonetheless, the radius may influence the final image. For example, in Fig. 9, the blue circles on the left represent the actual segmentation using the proposed closing. For this task, the *opt_closing* algorithm developed is not useful, although it has been demonstrated to work for the closing of the brain. As can be seen in the figure, there are certain gaps that even increasing the radius would remain as holes to fill using the algorithm. This happens due to the fact that the analysis is done parallel to the four sides, and in more directions. Therefore, it would have to be used for circular-like shaped structures like the brain.

Following the same Fig.9, since there is a small gap in the horizontal direction (small blue circle to the left), the program will try to fill it by increasing the radius. Thus, the section of the nose (big blue hole in the left image) takes part of the background. On the contrary, if we would like to apply a smaller radius the nose would be perfectly contoured (big hole on the right image) but more sections of the head with similar intensities than the background would be covered (small hole on the right image). In this sense, some pixels within the head have similar intensities to that of the background, mainly those of the cavities filled with air such as the mandible. Consequently, those sections are segmented by the Otsu method too, and the optimal closing might not be useful to close them.

Moreover, the following extraction of the brain mask proved an accurate segmentation of the whole brain, seen in Fig. 5. The process of obtaining the binary mask of the brain only needed two steps. They operated properly because the erosion was capable of differentiating the skull from the brain.

However, there were two images in which the erosion was rather too high or too low (Fig.11). This would end up in the segmentation of just one side of the brain (left), or a segmentation of the brain with a section of the skull (right). The images provided are 2D images sectioned from 3D images. In this sense, images like the one on the left of the figure have a better-joined brain in sections closer to the central part. Therefore, the use of a 3D structure is the most optimal way of determining the parameters/methods of use, since the analysis of a 2D layer out of a 3D volume is insufficient. The same phenomenon explains the wrong segmentation on the image to the right.

Then, the brain was chosen as the biggest region in all of the images, and it was followed by a dilation for balancing the previous erosion. Also, the optimal closing filled precisely the whole brain. Thus, is a fast technique that allows obtaining a brain mask.

On the other hand, the FCM clustering algorithm was able to acquire a significantly precise segmentation of WM and GM in every plane under study (see Fig. 13). Nonetheless, CSF was the worse segmented region of all. This is due to the fact that the CSF on the outer region was cropped by the brain mask, thus the FCM algorithm did not have enough information to properly cluster it. That is why in Fig. 13 the CSF is illustrated as a thin surrounding layer with almost unpredictable areas in the outer part. Despite this, there are some images where some anatomical regions are correctly segmented into CSF and WM, which is the case of the brainstem (see Fig. 12).

Followed by the brain segmentation, the skull stripping performance depended on that of all the previous segmentation. For that reason, it accumulates all the errors that the previous ones may had. However, the brain segmentation and background segmentation (Fig. 12) masks are accurate with respect to the images. In this sense, the skull is correctly segmented.

However, the space between the skull higher intensities (bone) and the contour of the brain, which contains both CSF and skull (e.g., skin) have very similar intensities. Therefore, it is very hard to determine exactly whether a pixel corresponds to the CSF or the skull with the resolution of the images provided.

V. Conclusion

Firstly, the preprocessing steps applied for the background removal are proven to work effectively on removing the noise artifact around the skull. Also, on correcting the bias field effect.

Secondly, the segmentation of the different tissues has shown to work properly for the three types of images. However, the small size (and so image resolution) of the

provided images and the fact that they are 2D slides of a 3D volume are drawbacks hardly solvable. They end up in the wrong segmentation of the brain, taking either sections of the skull or separating the lobes. Moreover, they prevent the FCM to locate precisely the CSF.

Thirdly, our proposed method has a low computational load, leading to a short time of execution. This is beneficial for the clinical setting and the management of large datasets.

For further lines of research, a dataset containing 3D images with higher resolution should be used. Moreover, the skull stripping could be improved by developing an algorithm that tracks the shape of it for improving CSF detection. Also, for a better generalization of the proposed method and its parameters, it should be validated using external datasets.

References

[1] Ivana Despotović, Bart Goossens, and Wilfried Philips. "MRI segmentation of the human brain: challenges, methods, and applications". In: *Computational and mathematical methods in medicine* 2015 (2015).

[2] Ewald Moser et al. "Magnetic resonance imaging methodology". In: *European journal of nuclear medicine and molecular imaging* 36.1 (2009), pp. 30–41.

[3] Mohd Ali Balafar et al. "Review of brain MRI image segmentation methods". In: *Artificial Intelligence Review* 33.3 (2010), pp. 261–274.

[4] Katherine L Perdue and Solomon G Diamond. "T1 magnetic resonance imaging head segmentation for diffuse optical tomography and electroencephalography". In: *Journal of biomedical optics* 19.2 (2014), p. 026011.

[5] Lei Hua et al. "A novel brain MRI image segmentation method using an improved multi-view fuzzy c-means clustering algorithm". In: *Frontiers in Neuroscience* 15 (2021), p. 662674.

[6] Magudeeswaran Veluchamy and Bharath Subramani. "Brain tissue segmentation for medical decision support systems". In: *Journal of Ambient Intelligence and Humanized Computing* 12.2 (2021), pp. 1851–1868.

[7] K Somasundaram and P Kalavathi. "Skull stripping of MRI head scans based on 2D region growing". In: *Proc. ICOM11 Tiruchirappalli, Tamil Nadu* (2011), pp. 18–23.

[8] Shuang Song, Yuanjie Zheng, and Yunlong He. "A review of methods for bias correction in medical images". In: *Biomedical Engineering Review* 1.1 (2017).

[9] Iza Sazanita Isa et al. "Evaluating denoising performances of fundamental filters for T2-weighted MRI images". In: *Procedia Computer Science* 60 (2015), pp. 760–768.

[10] R. Siva Kumar. "Performance analysis of image filtering algorithms for MRI images". In: *International Journal of Research in Engineering and Technology* 03 (2014), pp. 438–440.

[11] M.JAYAMANMADHARAO, Chinta Someswararao, and K. Reddy. "IMPLEMENTATION OF OBJECT ORIENTED APPROCH FOR NOISE REDUCTION USING FUZZY LOGIC". In: *International Journal of Engineering Science and Technology* 3 (Mar. 2011).

[12] Nicholas J Tustison et al. "N4ITK: improved N3 bias correction". In: *IEEE transactions on medical imaging* 29.6 (2010), pp. 1310–1320.

[13] Jae S Lim. "Two-dimensional signal and image processing". In: *Englewood Cliffs* (1990).

[14] Nobuyuki Otsu. "A threshold selection method from gray-level histograms". In: *IEEE transactions on systems, man, and cybernetics* 9.1 (1979), pp. 62–66.

[15] Jean Serra and Luc Vincent. "An overview of morphological filtering". In: *Circuits, Systems and Signal Processing* 11.1 (1992), pp. 47–108.

[16] Regina Pohle and Klaus D Toennies. "Segmentation of medical images using adaptive region growing". In: *Medical Imaging 2001: Image Processing*. Vol. 4322. SPIE. 2001, pp. 1337–1346.

[17] Chunming Li et al. "MRI Tissue Classification and Bias Field Estimation Based on Coherent Local Intensity Clustering: A Unified Energy Minimization Framework". In: vol. 21. Feb. 2009, pp. 288–99. ISBN: 978-3-642-02497-9. DOI: 10.1007/978-3-642-02498-6_24.

[18] Kelly H Zou et al. "Statistical validation of image segmentation quality based on a spatial overlap index1: scientific reports". In: *Academic radiology* 11.2 (2004), pp. 178–189.